8-2014

Numerical Investigation of the Nonlinear Dynamics of a Hybrid Acousto-optic Bragg Cell with a Variable Feedback Gain

Monish Ranjan Chatterjee
University of Dayton, mchatterjee1@udayton.edu

Hao Zhou
University of Dayton

Numerical Investigation of the Nonlinear Dynamics of a Hybrid Acousto-Optic Bragg Cell with a Variable Feedback Gain

Monish R. Chatterjee* and Hao Zhou

Department of Electrical & Computer Engineering

University of Dayton, Dayton, OH 45469

*Corresponding author

Email: mchatterjee1@udayton.edu; Tel.: (937) 886 2427

Abstract

Since around 1979, the operation of an acousto-optic Bragg cell under positive first-order feedback via amplification and delay in the loop has been studied extensively by several groups [1-3]. In recent work, the analysis of the nonlinear dynamics (NLD) of the system was extended to include bistable maps and Lyapunov exponents, and application of the chaos for signal encryption and decryption for uniform plane waves. The present work originated with the problem of a variable photodetector aperture opening relative to the first-order light. This potentially complex problem is simplified by assuming instead a variable feedback gain ($\tilde{\beta}$ (t)), which leads to considerably different NLD. This paper examines initially the NLD versus the (DC) bias voltage for different variable-$\tilde{\beta}$ conditions, including slow and fast rates of change of the gain with time in relation to the feedback delay. It is found that the response depends critically on the rate of rise of the feedback gain, and also that the resulting chaotic regimes are generally significantly different from those for fixed values of $\tilde{\beta}$. We have generated constant feedback gain $\tilde{\beta}$ and the variable feedback gain $\tilde{\beta}$ (t) chaos characteristics of the hybrid A-O network. Chaos as an equivalent carrier has been used to encrypt messages for both fixed and variable $\tilde{\beta}$. The transmitted signal is detected from the encrypted carrier using a heterodyne method, using a slave Bragg cell with matched keys to generate local chaos followed by a low pass filter and a phase inverter. Results between variable- and fixed-gain systems are compared in terms of advantages and disadvantages.

Keywords: A-O feedback, constant feedback gain, variable feedback gain, encryption, decryption, acousto-optic, bragg cell, nonlinear dynamics, time delay, passband, stopband.

1. Introduction

The present research focuses on an A-O Bragg cell with a first-order feedback. The output of the Bragg cell consists of zeroth- and first-order light beams. The first-order light beam is detected, amplified and fed back to the input. The time delay in the feedback makes the system nonlinear and complex in space-time analysis [4-5]. The time delay also introduces bistability in the hybrid A-O feedback (HAOF) device. Monostability, bistability, possible multistability and chaos in the hybrid A-O device may be obtained via three tuning effects viz., the feedback gain, time delay and the bias input [6-7].

Optics and Photonics for Information Processing VIII, edited by Abdul A. S. Awwal, Khan M. Iftekharuddin, Mohammad A. Matin, Andrés Márquez, Proc. of SPIE Vol. 9216, 92160V © 2014 SPIE
CCC code: 0277-786X/14/$18 · doi: 10.1117/12.2065316

Generation of A-O chaos involves careful tuning of the parameters and amplification of the feedback signal. Chaos waves may be used as a secure information carrier for transmitting data because of their random yet controlled nature. Modulation using chaos as a carrier wave was first attempted in the 1990s and many schemes have been designed to encrypt chaos waves using message signals with fewer numerical algorithms as encryption key than the classical methods [8-11]. The chaos wave may be viewed as a carrier which is subjected to a simple Amplitude Modulation (AM) scheme. Chaos may be viewed as a random disturbance that may be used to mask data from hackers. The basic random nature of chaos in the A-O case is inherent in its dependence on three factors viz. feedback gain, bias input and time delay that in effect protect the data. As discussed earlier, an A-O chaos system is governed by a key set of simple nonlinear differential equations that may be used to decrypt encrypted data transmitted over a channel. The resulting communication scheme using chaos as a carrier is similar in some respects to amplitude modulation, and therefore we may use a heterodyne scheme at the receiver for demodulation. The transmitter consists of a master chaos generator, a message generator and a device to encrypt the information on to the chaos carrier. The demodulation is conceptually similar to that of simple amplitude demodulation. The receiving scheme involves generating a chaos carrier with same characteristics as that of the input and using it via heterodyne to retrieve the information sent. Thus, the receiver system consists of a slave chaos generator (usually has the same characteristics as that of the transmitter) that generates the chaos carrier with the same frequency as that of the transmitted chaos carrier, a multiplier and a filtering device to filter out the unnecessary components in the output. In this paper, a variable gain amplifier is inserted in the feedback loop as an equivalent representation of a photodetector with time-varying aperture opening. The effect of a variable feedback gain studied in terms of slow and fast rate of change of the gain in the loop relative to the total feedback delay time. The optimal variable gain system is then examined for its NLD, chaotic regimes, passbands, and finally encryption and decryption properties. The numerical results are compared with those for a fixed-gain hybrid acousto-optic feedback (HAOF) system, and potential advantages identified.

2. Overview of the HAOF system

An acoustic wave is generated by applying an RF signal to a piezoelectric transducer that is suitably bonded to a crystal. The sound wave acts like a phase grating. An equivalent figure of merit Q similar to the quality factor in electrical resonance was introduced by Klein and Cook [12] that explains the diffraction in different A-O regimes. Q is given by

$$Q = \frac{LK^2}{k} = \frac{2\pi\lambda_0 L}{n\Lambda^2} = \frac{2\pi\lambda_0 L\Omega^2}{nv_s^2} \ , \tag{1}$$

Q is an important figure of merit which determines the regime of operation of an A-O modulator. When Q is close to 0, the system operates in the Raman-Nath regime, while 8π, the system operates in the Bragg regime. In Bragg regime when the light is incident at an angle (θ_B) called the Bragg angle, the light undergoes diffraction and generates first- and zeroth-orders as mentioned above. Most experiments involving A-O feedback assume operation in the Bragg regime. Around 1978, it was discovered that an A-O network with positive feedback exhibits bistability and hysteresis characteristics [2]. In refs [3] and [4] Chrostowski et.al used equivalent circuit models of the Bragg regime to demonstrate A-O bistabiolity. The standard Bragg cell transmitter with feedback is shown in Fig.1.

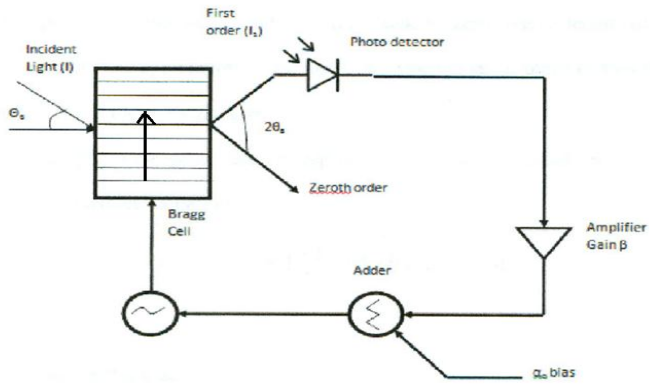

Fig.1. A-O Modulator with RF bias.

As shown in Fig.1, a beam of light is incident at an angle θ_B on a Bragg cell modulator, which in turn is modulated by an RF ultrasonic wave traveling through the Bragg cell. The incident light is diffracted into the first-order (intensity I_1) that is detected by a photo detector at the output, amplified and then fed back to the adder in the feedback loop. A plot of the first-order intensity vs. the bias input ($\hat{\alpha}_0$) shows the monostability, bistability and chaotic conditions of the modulator. The operating region of an A-O modulator depends on three *keys*: feedback gain $\tilde{\beta}$, input bias ($\hat{\alpha}_0$) and the time delay (TD).

With feedback plus time delay, the corresponding first-order detected intensity follows the nonlinear dynamical equation for uniform incident light and plane waves of light and sound:

$$I_1(t) = I_{inc} \sin^2[\frac{1}{2}(\hat{\alpha}_0(t) + \tilde{\beta}\, I_1(t - TD))] \ . \tag{2}$$

3. Simulation results for fixed and variable feedback gain

(a) Fixed gain $\tilde{\beta}$

An A-O system operates in monostable, bistable and chaotic regions depending on the bias input as was discussed earlier. Fig.2. summarizes the standard HAOF regimes.

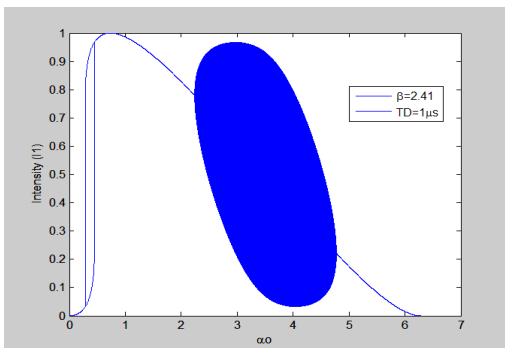

Fig.2. Different states of chaos.

Fig.2 shows different regions on the intensity vs bias input graph. Fig.2 indicates the lower monostable region where the first-order intensity has only one stable value for $\hat{\alpha}_0$ bias input. This is followed by the bistable region where the first-order intensity has two stable values for any single value of bias input. The system again enters a monostable region called the upper monostable region where the first-order intensity assumes a single value. Then the system enters chaos and undergoes multiple random oscillations. From the figure it is evident that the chaos starts after a particular (threshold) value of $\hat{\alpha}_0$ bias called $\hat{\alpha}_{Th}$ (after $\hat{\alpha}_0$ =2 from Fig.2).

When we increase feedback gain $\tilde{\beta}$ to 3, the resulting NLD is as shown in Fig.3.

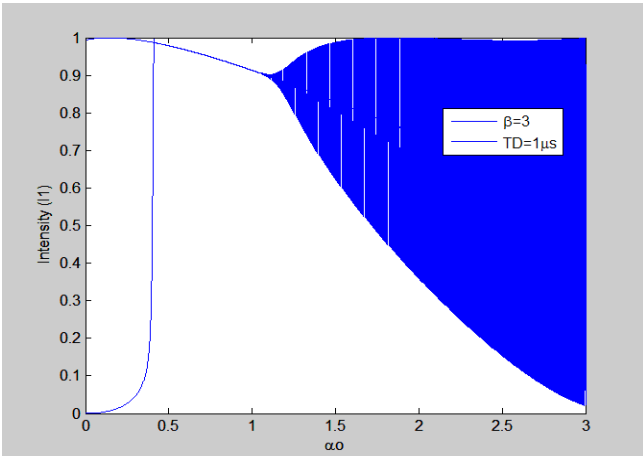

Fig.3. Chaos of feedback gain $\tilde{\beta}$ is 3.

Fig.3 shows certain differences from Fig.2. The lower monostable region has almost disappeared. The bistable region where the first order intensity has two stable values for any single value of bias input has become wider. The system again enters the upper monostable region where the first order intensity assumes a single value. Then the system enters chaos and undergoes mutiple random oscillations earlier than Fig 2. This shows that a change of feedback gain $\tilde{\beta}$ leads to significant changes in the HAOF system. Also, the domain of chaos is much broader, and takes on a manta ray shape versus $\hat{\alpha}_0$. As was seen from Fig.2, chaos starts after a particular value of $\hat{\alpha}_0$ bias called $\hat{\alpha}_{Th}$. By varying the value of $\hat{\alpha}_0$ in discrete steps of 0.1 from from 1.0 to 1.5, it is found that the closed loop response reaches a monostable steady-state from about 50TD to about 150TD for $\hat{\alpha}_0$ upto 1.2; thereafter, for larger values of $\hat{\alpha}_0$, the closed loop enters chaos and does not acquire steady state at all. Three such results are shown in Figs. 4-6 corresponding to $I_{inc} = 1, I_1(0) = 0$, and $\tilde{\beta}$ =3, time delay (TD) is 1 μs. While Fig.4 shows steady state acquired in 50TD, Fig.5 shows onset of chaos around 150TD; when $\hat{\alpha}_0$ is increased to 1.5 as in Fig.6, the system enters chaos with virtually no build-up or onset time.

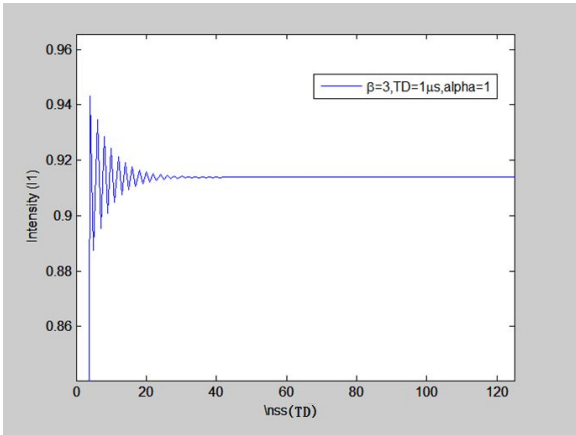

Fig.4. Monostable acquisition for $\hat{\alpha}_0$ =1.

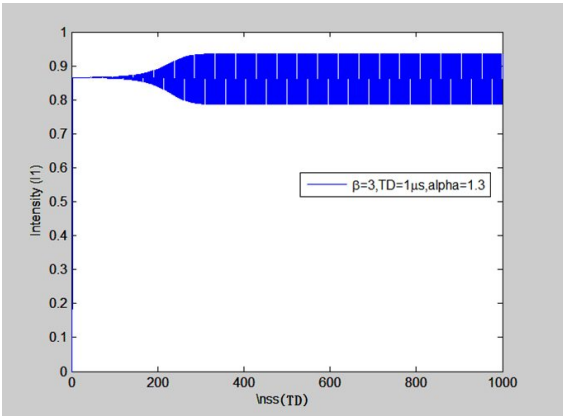

Fig.5. Onset of chaotic oscillations for $\hat{\alpha}_0$ =1.3.

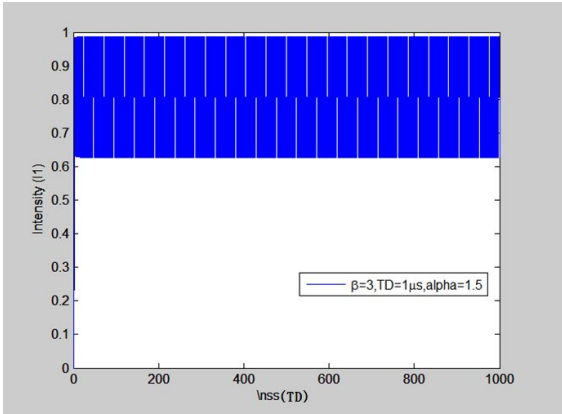

Fig.6. Persistence of chaotic oscillations for $\hat{\alpha}_0$ =1.5.

As seen from Figs.4-6, when $\hat{\alpha}_0$ is increased to 1.3, the system clearly enters chaos and there is no settling time as seen from Fig.7. When $\hat{\alpha}_0$ is increased to 1.5, chaos commences from almost t = 0.

Fig.7 shows time oscillations of a chaos wave when its feedback gain $\tilde{\beta}$ is 3 and $\hat{\alpha}_0$ bias is 3.5 for a TD=1 μs . Fig.8 shows a snapshot of Fig.7 with the detailed oscillations.

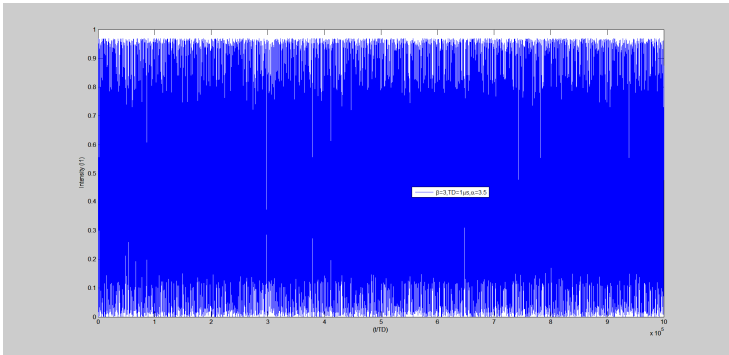

Fig.7. Chaos frequency of t=10^6 TD=1s (TD= 1 μs).

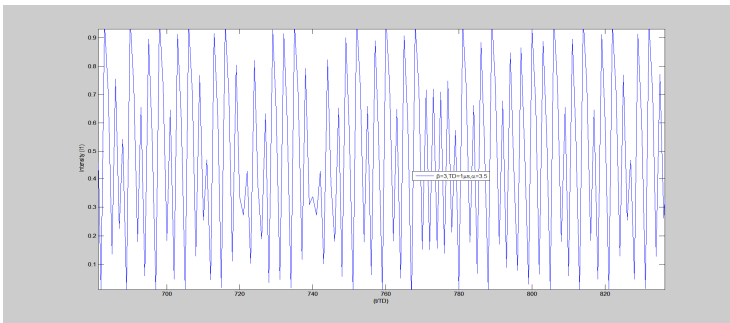

Fig.8. Snapshot chaos frequency of t=10^6 TD=1s (TD= 1 μs).

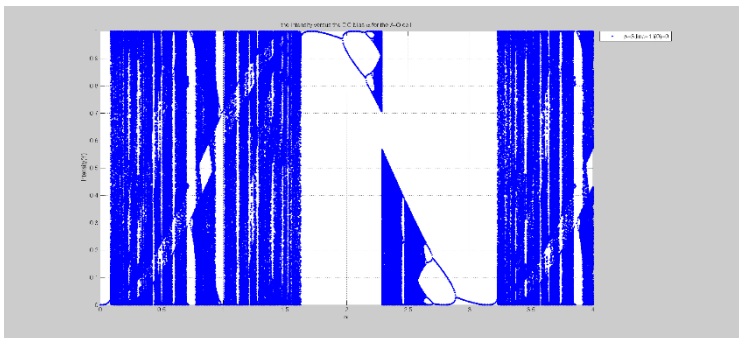

Fig.9. The bifurcation map of of . $I_{inc} = 1, I_1(0) = 0, and\ \tilde{\beta} = 3$.

The blue regions in Fig.9 indicate chaotic passbands where chaos occurs while the white regions indicate stopbands where the system is non-chaotic. The bifurcation results match well with the known fact that for $\hat{\alpha}_0$ = 3.5, the system obviously exhibits chaotic oscillations (as in Fig.7) which is in a chaotic

passband (as in Fig.9). Thus, the results are compatible. As a sidelight, we observe that the extended stopband in Fig.9 is reminiscent of the Northwestern University logo.

(b) Variable gain $\tilde{\beta}$ (t)

The system shown in Fig.1 represented the standard Bragg cell transmitter with feedback. We next consider the case where instead of capturing all the incident light, the photo detector happens to have a variable aperture which may open and close with time. This variable photocurrent situation is comparable to an equivalent system described by a fixed aperture with a *variable* feedback gain .

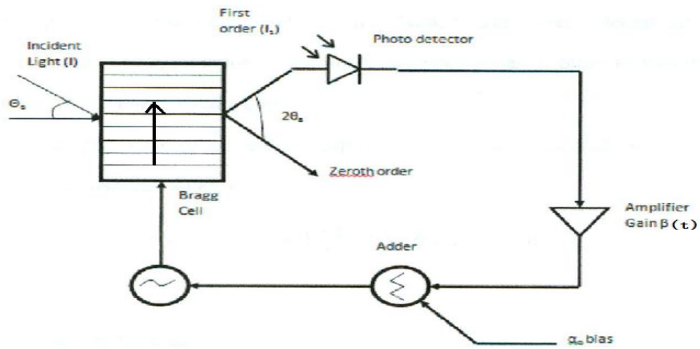

Fig.10. A-O Modulator with RF bias under variable feedback gain.

In the initial tests of the system in Fig.10, a variable feedback gain $\tilde{\beta}(t)$ increasing with time as in Fig.11 was used to examine its NLD. Several trials indicated that the rate of rise of $\tilde{\beta}(t)$ *relative to the delay* TD *in the feedback loop* is critical to the closed-loop NLD of the system. Too slow a rate of rise leads to results no different from that for constant $\tilde{\beta}$, while a rate too fast prevents the system from entering chaos. A workable solution was found to be where the variable feedback gain $\tilde{\beta}(t)$ rises as a ramp from 0 to 10000TD, within which the gain increases from 2.8 to 3.2.

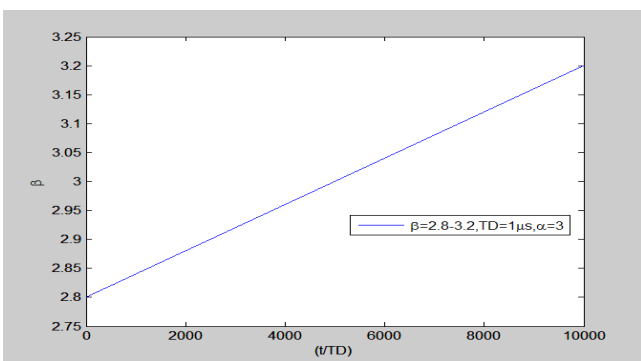

Fig.11. Feedback gain $\tilde{\beta}(t)$ increase by time.

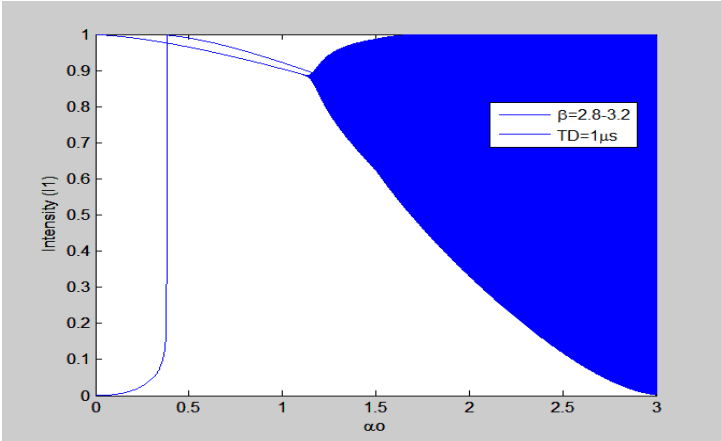

Fig.12. Chaos of variable feedback gain $\tilde{\beta}(t)$.

Fig.12 shows that the lower monostable region almost disappears compared with what was seen in Fig.2. The bistable region where the first order intensity has two stable values for any single value of the bias input is wider. Then the system enters chaos and undergoes multiple random oscillations similar to Fig.3. This shows that a variable feedback gain $\tilde{\beta}(t)$ leads to changes in the A-O chaos characteristics. Figs.14 and show that a variable $\tilde{\beta}$ yields chaos in the NLD of the HAOF system for lower values of the lower limit of the gain. Fig.13 shows a time snapshot for chaotic oscillations in a HAOF with variable feedback gain $\tilde{\beta}(t)$ (from 2.8-3.2) with $\hat{\alpha}_0$ bias at 3.5 and TD=1 μs .

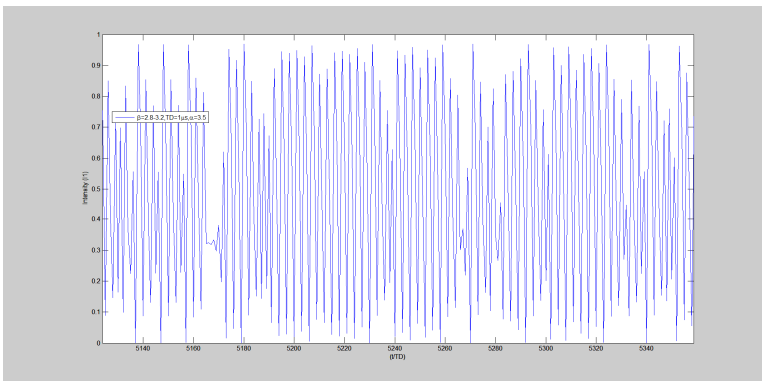

Fig.13. Snapshot variable feedback gain chaos frequency of t=10^6 TD=1s (TD= 1 μs).

Shown in the figures that follow are the bifurcation maps for different variable feedback gain ramps. Fig.14 is closest to Fig.9 which was the bifurcation map for a constant feedback gain (the white stopbands like the Northwestern logo). Thus a smaller range of $\tilde{\beta}$ variations creates relatively small variations in the chaotic behavior. In Fig.16 the left pillar of the Northwestern logo has virtually disappeared (thus there is mostly a sea of blue passband, with only a narrow white pillar representing the stopband- likely approaching the University of Dayton logo). Fig.15 exhibits intermediate characteristics with the $\tilde{\beta}$ range 2-4. These results indicate that a slow rise of $\tilde{\beta}(t)$ over a wider amplitude range leads to a reduction of stopbands and a corresponding increase in the extent and bandwidth of the passbands.

This would potentially increase the dynamic range of AC signals used in encryption applications. Parameter tolerance would need further evaluation.

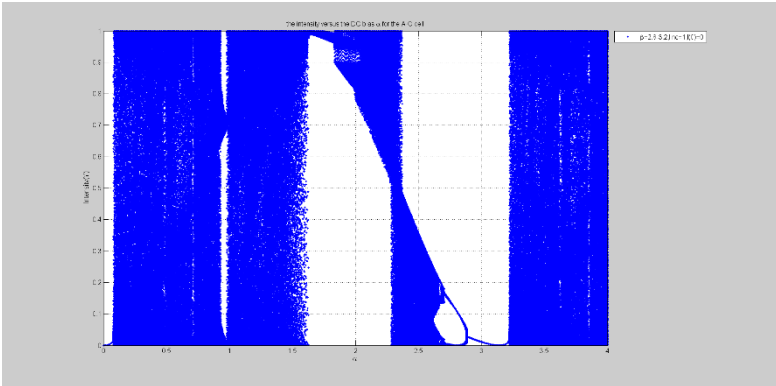

Fig.14. The bifurcation map of of $I_{inc} = 1, I_1(0) = 0, and\ \tilde{\beta}(t) = 2.8 - 3.2$.

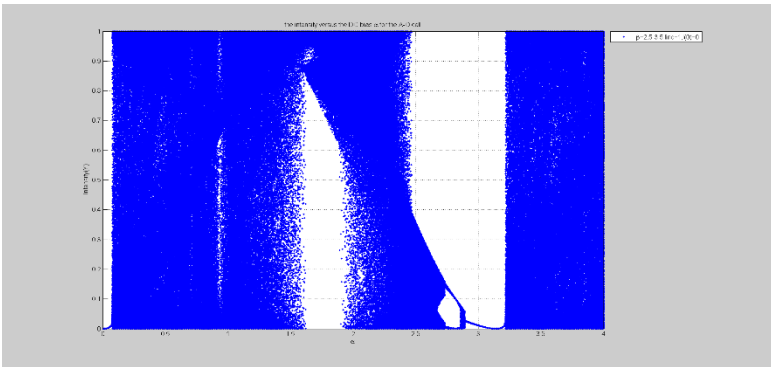

Fig.15. The bifurcation map of of $I_{inc} = 1, I_1(0) = 0, and\ \tilde{\beta}(t) = 2.5 - 3.5$.

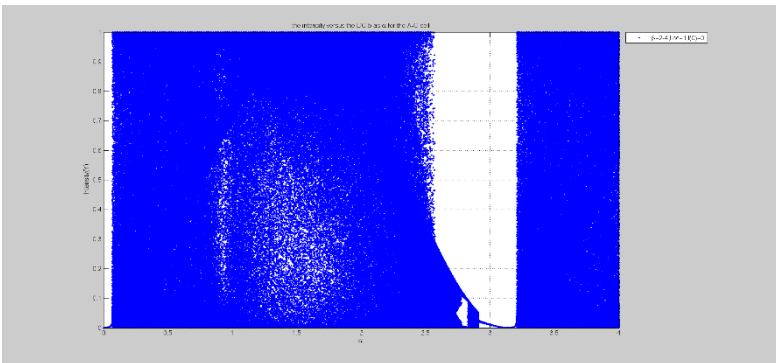

Fig.16. The bifurcation map of $I_{inc} = 1, I_1(0) = 0, and\ \tilde{\beta}(t) = 2.0 - 4.0$.

4. Chaotic signal encryption and decryption and the information security of the variable feedback gain

It was E.N Lorenz in 1963 who first found that in a set of three differential equations with non-periodic solutions, the solutions underwent irregular fluctuations, and were bounded but unstable [23].

But the term chaos for these observed irregular periodic oscillations was first termed by Poincare [24]. Encryption scheme in a chaotic system also follows the regular amplitude modulation (AM) for analog signals. It involves choosing a carrier close to chaos frequency f_c and then encrypt the message on that carrier. The decoding at the receiver is similar to the heterodyne scheme used in the AM demodulation involves generating a local chaos carrier wave, then multiplying the local chaos wave with the received "chaos + message" signal and low pass filtering the product to filter out the high frequency carrier and retaining the low frequency message. The viability of such a concept in the context of acousto-optic chaos has been demonstrated in recent work [15].

As mentioned in ref. [4], bistability and possible chaos depend on the choice of the feedback gain $\tilde{\beta}$, input bias($\hat{\alpha}_0$) and the time delay (TD) in the loop. Chaotic encryption is accomplished by adding a message signal to the dc bias input and the feedback input at the transmitter driver circuit, as shown in Fig.17. The receiver consists of a slave hybrid A-O circuit that generates a chaos wave that is in synchronization with the master hybrid A-O device used to generate the chaos wave used for encrypting message at the transmitter. The locally generated chaos at the receiver is then multiplied with received chaos plus message signal, then low pass filtered to extract the message signal.

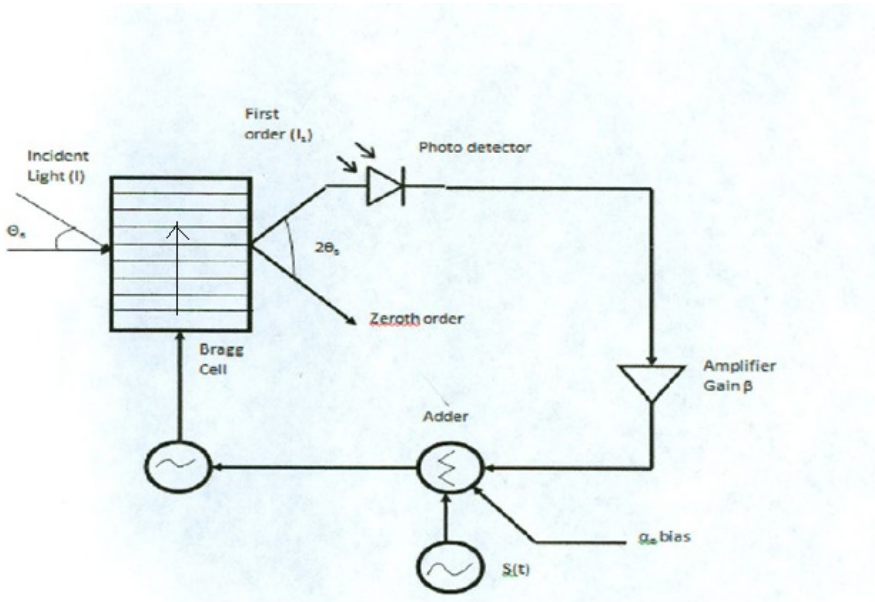

Fig.17. Chaotic encryption in HAOF.

As was explained earlier encryption is done by adding ac message signal to the dc bias input $\hat{\alpha}_0$, at the adder which is then fed as input to the piezoelectric transducer which generates the RF input for the Bragg cell. Because of the chaotic nature of the carrier the message signal is encrypted on the carrier and transmitted as shown in Fig.17.

The choice of $\hat{\alpha}_0$ is crucial for encryption on the chaotic carrier. From nonlinear analysis and bifurcation graphs of chaos vs different parameters that effect the chaos (such as the feedback gain $\tilde{\beta}$, input bias($\hat{\alpha}_0$) and the time delay (TD)), it is known that there are specific passbands within which chaos

exists for a given set of parameters or *keys*. Fig.9 shows the blue chaotic passbands versus $\hat{\alpha}_0$ on the bifurcation map for a fixed $\tilde{\beta}$. Based on these findings, all the encryption experiments reported in this paper have been performed around $\hat{\alpha}_0 = 3.5$, and $\hat{\alpha}_{ac} = 0.25$ has been chosen as the peak signal amplitude been chosen to ensure that the net bias voltage lies within the passband range of 3.25 to 3.75. Thus, for the encryption $3.25 < \hat{\alpha}_{total} < 3.75$. Fig.18 shows the schematic of the chaotic demodulator used for decrypting the secure signal.

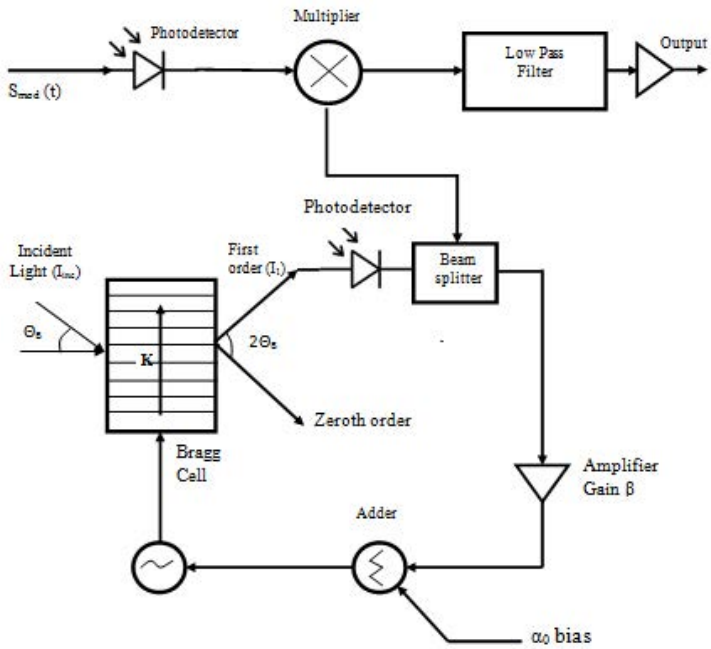

Fig.18. Chaotic decryption in a receiver HAOF (after ref. [16]).

Fig.19 shows the NLD of the HAOF with sinusoidal encryption. The modulation appears to introduce a wave-like envelope to the manta ray profile of Fig.3.

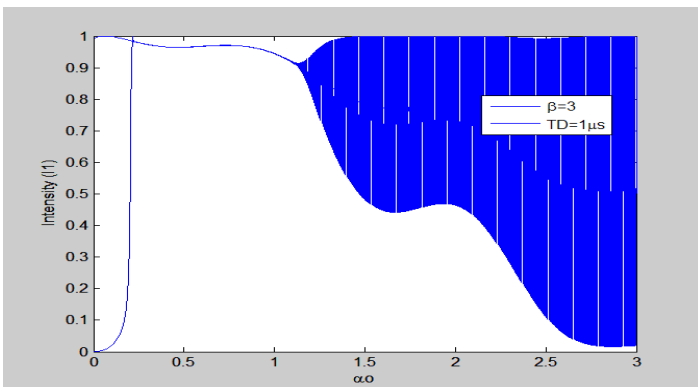

Fig.19(a). NLD of HAOF with constant feedback gain β and sinusoidal signal.

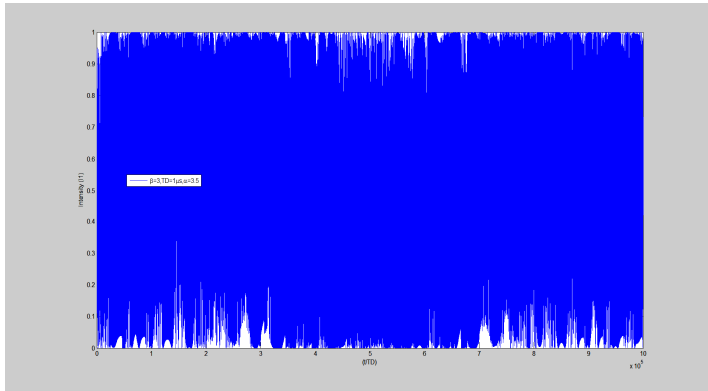

Fig.19(b). Constant feedback gain chaos encrypted by a modulated sine wave.

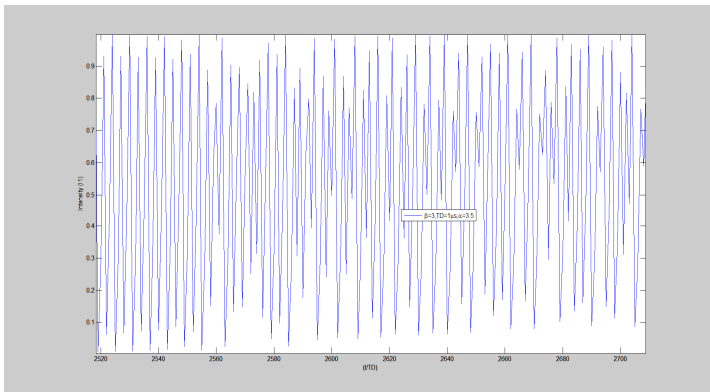

Fig.19(c). Time snapshot of constant feedback gain chaos encrypted by a sine wave.

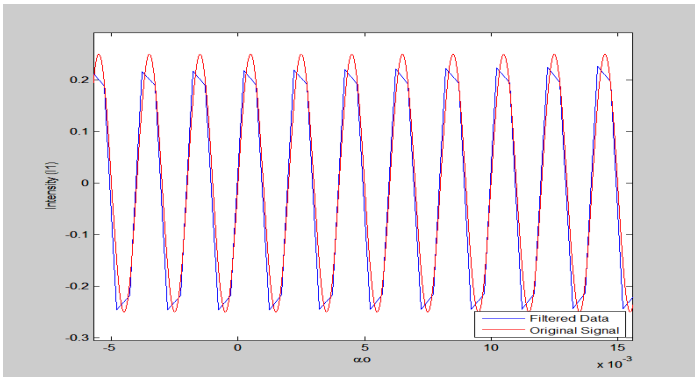

Fig.19(d). Superposed filtered data and original signal for sinusoidally encrypted chaos.

Figs.19(a-d) show the NLD, the sinusoidally encrypted chaos, its zoomed time waveform, and the original and recovered output from the demodulator for a case of a fixed $\tilde{\beta}$ of 3.0.

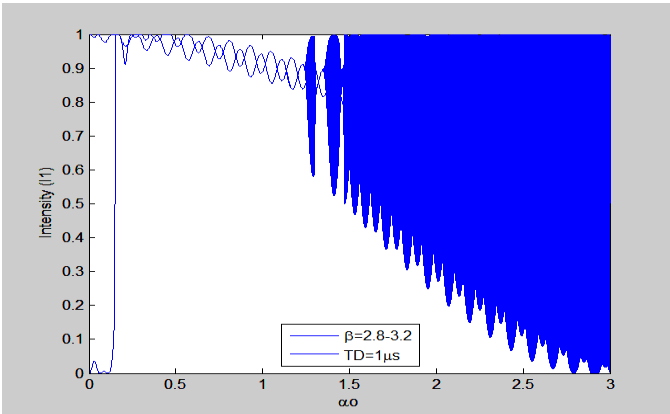

Fig.20(a). NLD of HAOF system with sinusoidal modulation for variable feedback gain $\widetilde{\beta}(t)$.

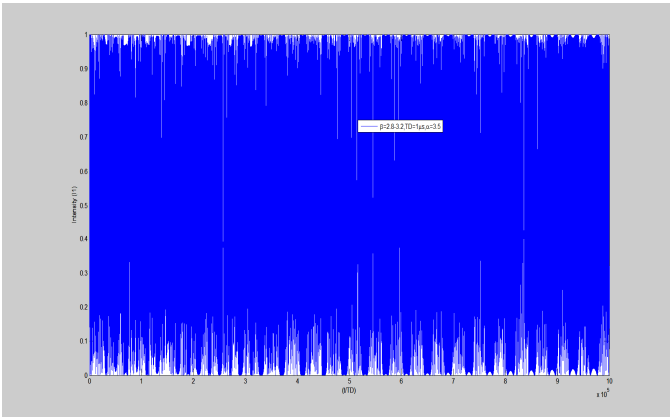

Fig.20(b). Wave of encrypted chaos with sinusoidal modulation for variable feedback gain $\widetilde{\beta}(t)$.

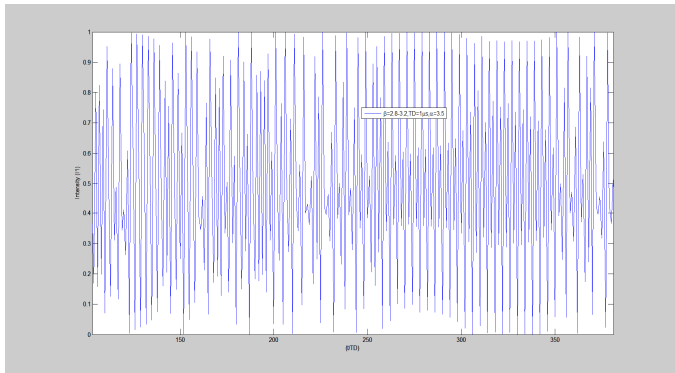

Fig.20(c). Time snapshot of a zoomed detail of Fig.21(b).

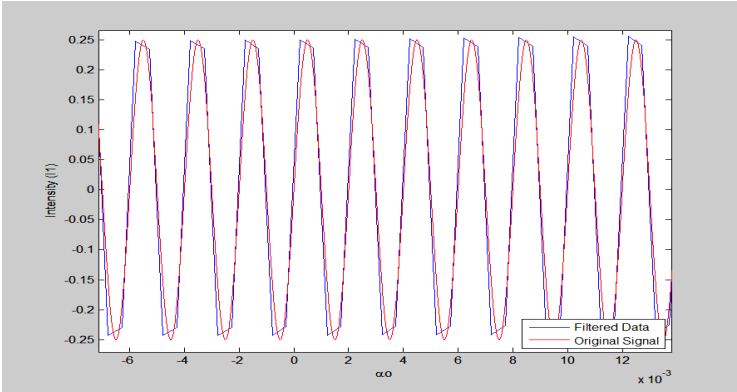

Fig.20(d). Superposed filtered data and original signal for sinusoidally encrypted chaos with variable gain.

Figs.19(a-d) and 20(a-d) demonstrate that AC signal modulation and retrieval with reliable encryption is possible for the case of a variable feedback gain provided an appropriate rate of rise is selected for the gain. The variable gain approach may likely also have the advantages of greater signal dynamic range and possibly tighter parameter tolerance.

5. Conclusion and further work

This research focused on the optical characteristics of a hybrid A-O feedback device with variable gain. We have generated chaos and allied conditions corresponding to constant and variable feedback gain $\tilde{\beta}(t)$, and studied in detail the NLD of the two systems. The generation of chaos has been studied for different parameters such as feedback gain $\tilde{\beta}$, input bias($\hat{\alpha}_0$) and the time delay (TD). Additionally, the variable gain system has been designed for applications to signal encryption and decryption utilizing modulated chaos waves with uniform incident plane waves. A receiver scheme has been developed using a second Bragg cell with matched bias parameters to generate local chaos followed by a low pass filter. This heterodyne system then extracts the securely transmitted message. It is generally observed that the chaotic system experiences more passband and stopband transitions for comparable system parameters relative to a fixed- $\tilde{\beta}(t)$ problem. This research provides some insight into the NLD of variable feedback, and potentially holds out the promise that the resulting system when properly designed may offer higher system robustness, and also greater dynamic ranges for information under transmission.

Acknowledgment

The authors would like to thank Fares Almehmadi for assistance with this work at various stages.

References

1. J.Chrostowski and C. Delisle, "Bistable piezoelectric Fabry-Perot interferometer," Can. J. Phys. 57, 1376-1379 (1979).
2. J.Chrostowski and C. Delisle, "Bistable optical switching based on Bragg diffraction," Opt. Comm. 41, 71-74 (1982).
3. J.Chrostowski, C. Delisle and R. Tremblay, "Oscillations in acousto-optic bistable device," Can. J.Phys. 61, 188-191 (1983).

4. R.Valle, and C. Delisle, "Route to chaos in an acousto-optic bistable device," Phys. Rev. A 31, 2390-2396 (1985).
5. L.Larger, J-P Goedgebuer and F. Delmore, "Optical encryption system using hyperchaos generated by an optoelectronic wavelength oscillator," Phy. Rev. 57, 6618-6624 (1998).
6. C. Mirasso, R. Vicente, P. Colet, J. Mulet, and T. Perez, "Synchronization properties of chaotic semiconductor lasers and applications to encrypyion," C.R. Physique 5, 613-622 (2004).
7. A.Korpel, "Acousto-optics," 2nd ed., Marcel Dekker: New York (1997).
8. P. Debye and F.W. Sears, "On the scattering of light bysupersonic waves," Proc. Nat. Acad. Sci. 18, 409-414 (1932).
9. R. Lucas and P. Biquard, "Optical properties of solid and liquid medias subjected to high-frequency elastic vibrations," Jour. De. Phys, et Rad. 3, 464-477 (1932).
10. A. Korpel, "Selected Papers on Acousto-Optics," SPIE Milestone Series 16, 73-78 (1990).
11. W.L. Bragg, "The Diffraction of Short Electromagnetic Waves by a Crystal," Proc. Camb. Phil. Soc. 17, 43-75 (1913).
12. W.R. Klein and B.D. Cook, "Unified approach to ultrasonic light diffraction," IEEE Trans. Sonics Ultranson. SU-14, 123-133 (1967).
13. E.N. Lorenz, "Determinnisitic non-periodic flow," J. Atoms. Sci. 20, 130-141 (1963).
14. T.Y. Li and J.A. Yorke, "Period three implies chaos," Am. Math. Monthly 82, 985-992 (1975).
15. M. R. Chatterjee and M. A. Al-Saedi, "Examination of the nonlinear dynamics of a chaotic acousto-optic Bragg modulator with feedback under signal encryption and decryption," Opt. Eng. 51(1) 018003 (2012).
16. A. Kundur, *MSEE Thesis*, University of Dayton (May 2012).